From Powder Manufacturing to Perovskite/*p*-type TCO Thin Film Deposition

YOUSSOUF DOUMBIA [ID],[1,4] AMAL BOUICH,[1,3] ABDOULAYE TOURÉ,[1]
JÚLIA MARÍ GUAITA,[1] BERNABÉ MARI SOUCASE,[1]
and DONAFOLOGO SORO[2]

1.—Institut de Disseny per a la Fabricació i Producció Automatitzada, Universitat Politècnica de València, 46022 València, Spain. 2.—Département des Sciences et Technologie, Ecole Normale Supérieure (ENS) d'Abidjan, BP 10, Abidjan 08, Ivory Coast. 3.—Fisica Aplicada a las Ingenierias Aeronautica y Naval & Instituto de Energia Solar, Universidad Politécnica de Madrid, 28040 Madrid, Spain. 4.—e-mail: doumbiayoussouf59@yahoo.fr

Photovoltaic perovskites are very attractive candidates as absorber layers because of their very interesting properties. In the present work, we have two parts: first, we prepared powders of the perovskites $MAPbBr_3$, $MAPbI_3$, and $MAPbCl_3$, with the aim of maximizing their purity, and then we deposited thin films using these powders previously prepared by the one-step spin-coating method. The anti-solvent used was under the same ambient deposition conditions. We concluded with a series of characterizations such as X-ray diffraction, scanning electron microscopy, and UV–visible absorption to better appreciate the quality of the films produced. The crystalline structures of the films, their surface morphology, and their optical properties from the characterizations show that we have succeeded in producing film samples suitable for photovoltaics.

INTRODUCTION

In recent years, climate change, the reduction of fossil fuel sources, the inevitable increase in their price, the negative consequences of their use, and the growing demand for energy have all been arguments in favor of the development of renewable energy.[1–6] The fear of nuclear accidents is pushing countries to abandon or at least to reduce nuclear power plants. However, the availability of sufficient energy is an essential element for the development of mankind and is therefore a major problem for all nations. Solving this problem requires the development of new generation systems, the optimization of the modes of distribution of energy products, and their rational and efficient use. These three aspects are the basic pillars of any energy policy, with the requirement to have the least possible impact on the environment. The current energy scenario involves systems of increasing complexity, where the

solutions to be used must be continually reviewed in light of new results from energy research. This must address with the greatest possible intensity concrete projects that allow for the improvement of some of the four aspects mentioned above: greater production capacity, better distribution, maximum savings, and minimum environmental impact. We can say that, in the current situation, research on energy issues has become of paramount importance. It is in this context that research has been embarked into renewable energies in general, but especially in the field of solar photovoltaic energy. Indeed, in the field of photovoltaics, several technologies have been developed, the first of which is silicon technologies.[7–12] Silicon-based solar cells, which dominate the market today, have an energy yield of around 24%, which took more than 30 years of research and heavy investment to achieve. Depending on the manufacturing technology, the availability of materials for the production of solar cells, and the field of application, researchers have been interested in other types of cells, such as organic cells, metal oxides, and cadmium tellurium, to name but a few.[13–17]

The methods used to shape perovskite-based solar cells are gentler than those for crystalline silicon. Whereas silicon has to be heated to nearly 3000°C to crystallize it into a block, part of which is lost during the cutting process, perovskites use gentle methods, such as centrifugal coating or immersion coating, which are carried out at room temperature.

The nature of the halogen X in ABX_3 perovskites has an effect on the band gap width and stability of the material. In general, the smaller the halogen anion, the larger the band gap and the lower the stability of the material.[18,19] For example, $MAPbCl_3$ has a band gap of 3.1 eV, which corresponds to ultraviolet light absorption, with an orthorhombic structure. $FAPbBr_3$ has a band gap of 1.9 eV, corresponding to light absorption in the visible range. $MAPbI_3$ has a band gap of 1.55 eV, but has a cubic structure that is unstable at room temperature. The compounds used to synthesize halide perovskites are generally obtained by chemical reactions between precursors that are soluble in organic or aqueous solvents. For example, $MAPbI_3$ can be obtained by reacting methylammonium iodide with lead iodide PbI_2 in a solution of dimethylformamide (DMF) or dimethylsulfoxide (DMSO). The solution can then be deposited on a substrate and heated to form a thin layer of $MAPbI_3$. This is the solvent evaporation method, which involves depositing a solution containing the precursors of halogenated perovskites on a substrate and allowing the solvents to evaporate at room or slightly elevated temperature. It is quick and easy to use, as no intermediate steps are required. However, it can lead to poor reproducibility, poor quality thin films, and increased thin-film instability.

Another method, the pre-deposition powder preparation method, is more complex and time-consuming, but can produce high-quality thin films with good purity, crystallinity, and stability. The pre-deposition powder synthesis method involves preparing a powder of halogenated perovskites by chemical reactions in a solution or in solid state, then depositing this powder on a substrate and annealing it to form thin films.

Always on the lookout for materials with high efficiency and above all easy to elaborate, research led to the discovery of new materials called perovskite.[20–24] The light-absorbing layers, also known as active layers, from the first generation of cells to the third generation of cells, are currently expanding the horizons of photovoltaic solar cells.

Indeed, thanks to the efforts of researchers in the photovoltaic field to improve the performance of these absorbing layers, both in terms of optimization and research into new materials, we are seeing an evolution in the parameters of solar cells. It is thanks to these efforts that we have moved from conventional silicon cells (first generation) to third-generation perovskite thin films.[25–29] Organic lead halide perovskites of the general formula $APbX_3$

(A = methylammonium MA, formamidinium FA, cesium Cs, and X = Br, Cl, I, Br/Cl, Br/I and I/Cl) which are abundant, low cost, and well suited to converting solar energy into electricity as absorbers have had a very important impact in the field of photovoltaics.[24,30–36] This good impression of perovskites is due to their interesting characteristics, namely their high absorption coefficient and high mobility of charge carriers increasing the energy conversion efficiency from 3.8% in 2009 to currently 25.2%.[37–40] In addition to single lead halide perovskites, mixed halide perovskites ($MAPbX_{3-q}Y_q$ with $q = 0$, 1, 2, and 3, and X and Y different halogens) are also used for photovoltaic applications. Perovskite materials are also used for the fabrication of light emitters.[41–46] Although perovskites have many advantages, their main challenge remains their structural stability. It should be noted that organic lead halide perovskite thin films are usually made from precursors directly dissolved in solvents such as DMF and/or DMSO. In the present work, we are interested in the fabrication of the much purer $MAPbX_3$ (X = Br, Cl, and I) perovskite powder which we will then use to elaborate thin films in order to optimize the performance of the films. We present a study of the crystal structure, surface image, and optical absorption of the prepared thin films.

Transparent conducting oxides (TCOs) allow visible radiation to access or depart from a display while also supplying electrical connections due to their combination of strong electrical conductivity and optical transparency in the visible spectrum.[47–49] This is why they are essential components of many gadgets, including touchscreens and photovoltaic solar cells.[50–58] TCOs are classified into two categories, n-type and p-type. Several researchers have concentrated on n-type materials, such as ITO, FTO, and ZnO; Al or ZnO; or Ga. On the other hand, there has been less research on p-type materials, which is why they have not been developed.[59–67] By combining n-type and p-type materials in a p–n heterojunction, an outstanding production of oxides would be impacted by high-performance p-type TCOs.[68–70] The contribution of this work is to prepare powders of higher quality than the precursors usually used to make perovskite thin films. This could improve the optoelectronic properties of the films for use in photovoltaic solar cells.

MANUFACTURE OF POWDERS

The production of good-quality perovskite thin films by the one-step spin-coating method is generally carried out in two ways:

- Directly using pure precursors (A = MAX, FAX, and CsX; B = PbX_2, FAX_2, or CsX_2) dissolved in a solvent which can be DMF or DMSO. The prepared solution is then deposited on a suitable substrate.[71,72]

- First prepare the perovskite powder to be deposited and then dissolve it in DMF or DMSO to make the solution to be deposited.[73,74]

In this study, we opted for the second method, i.e., we prepared the powder for our perovskite thin films (MAPbBr$_3$, MAPbCl$_3$, and MAPbI$_3$).

Manufacture of MAPbBr$_3$

The manufacturing process of the perovskite powders is as follows.

We first put 50.57 g of bromidic acid (HBr, 99% purity) in a round-bottom flask with two nozzles (Fig. 1a). To this, we added 28.236 g of a methylamine solution (CH$_3$NH$_2$, 99% purity). It should be noted that, before adding the CH$_3$NH$_2$, the flask was placed in ice on a magnetic stirrer (about 200 rpm) to maintain the temperature at 0°C (Fig. 1b). Mixing the two solutions increased the temperature from 0°C to 100°C, when we added 50 mL (9.93 g) of lead nitrate (PbNO$_3$, 98% purity). When the temperature dropped to about 40°C, the mixture, which has precipitated, was filtered under vacuum (Fig. 1c). The mixture was rinsed 3–4 times with absolute ethanol and diethyl ether, still under vacuum, to remove all impurities, after which the powder obtained was weighed before being dried in an oven to remove any moisture (Fig. 1d and e). For the calculation of the yield (ξ), we obtained:

$$\xi = \frac{\text{Mass}_{\text{finale}}}{0.03 \times \text{Molar mass}_{(MAPbBr3)}}$$
$$= \frac{13.75 \text{ g}}{0.03 \text{ mol} \times 478.98 \text{ g/mol}} \times 100 = 95.68945\%$$

$\xi = 95.68945\%$, 0.03 mol corresponds to the amount of PbNO$_3$.

$$m(\text{HBr}) = \frac{0.3 \text{ mol} \times 80.9 \text{ M}}{0.48} = 50.57 \text{ g}$$

$$m(\text{CH}_3\text{NH}_2) = \frac{0.3 \text{ mol} \times 31.06 \text{ M}}{0.33} = 28.236 \text{ g}$$

$$m(\text{PbNO}_3) = \frac{0.03 \text{ mol} \times 331.2}{1} = 9.93 \text{ g}$$

Manufacture of MAPbCl$_3$ and MAPbI$_3$

The manufacturing process of MAPbCl$_3$ and MAPbI$_3$ powders, as well as the precursors, are the same as for MAPbBr$_3$, always with the same quantities, and same purity, except that, for MAPbCl$_3$, chloride acid (HCl solution, 99% purity) was used instead of bromidic acid (HBr solution, 99% purity), and for MAPbI$_3$, iodidric acid (HI solution, 99% purity) was used. For the yield of MAPbCl$_3$, we have:

$$\xi = \frac{\text{Mass}_{\text{final}}}{0.03 \times \text{Molar mass}_{(MAPbCl3)}}$$
$$= \frac{7.89 \text{ g}}{0.03 \text{ mol} \times 344.609 \text{ g/mol}} \times 100 = 76\%$$

$$m(\text{HCl}) = \frac{0.3 \text{ mol} \times 36.458 \text{ M}}{0.37} = 29.56 \text{ g}$$

For the performance of MAPbI$_3$. we have:

$$\xi = \frac{\text{Mass}_{\text{final}}}{0.03 \times \text{Molar mass}_{(MAPbI3)}}$$
$$= \frac{16.12 \text{ g}}{0.03 \times 619.109 \text{ g/mol}} \times 100 = 86\%$$

$$m(\text{HI}) = \frac{0.3 \text{ mol} \times 127.904 \text{ M}}{0.37} = 103.71 \text{ g}$$

The different steps in the manufacture of powders are summarized in Fig. 1. In Fig 1a, we have introduced the acid halide HX (X = Br, Cl, or I). We have then added methylamine MA to the HX solution, which had previously been placed on ice (Fig. 1b). The precipitate was filtered under vacuum to obtain the powder (Fig. 1c). Figure 1d shows the powder while still wet, and Fig. 1e shows them after oven-drying.
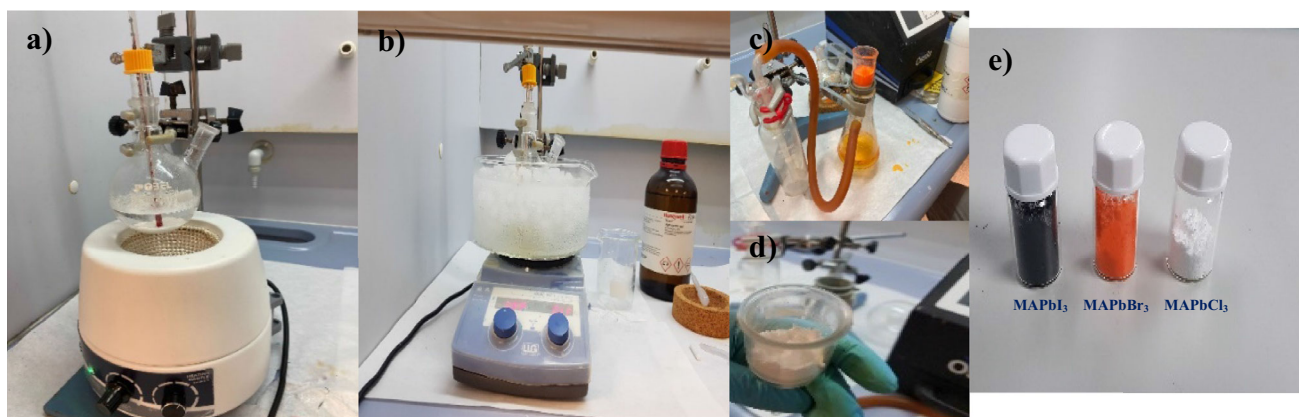

Fig 1. The powder manufacturing process.

ELABORATION OF THIN FILMS

Materials and Methods

We used a few grams of the different powders which we dissolved in DMF to obtain 1 mL of the solution to deposit. As a substrate, we opted for fluorine-doped tin oxide (FTO)-coated glass which was well treated in order to have good-quality thin films. The deposition method was a one-step spin coating with a rotation of 4000 rpm for 50 s. The films were then annealed on a hot plate at 80°C for 20 min. Figure 2 shows the development of the MAPbBr$_3$, MAPbCl$_3$, and MAPbI$_3$ perovskite thin films.

Instrumentation

Different characterization techniques are an essential means of studying the active layers of the photovoltaic solar cell and the cell as a whole. In this sense, they allow us to judge the relevance of our work through the data.

In this study, we have made the following analyses:

- X-ray diffraction (XRD) determines the crystallinity of the thin films developed and the crystallographic orientations. At the same time, this technique provides information on which layer has the best crystallinity. The range of diffraction angles 2θ was set between $10°$ and $60°$ using a RIGAKU Ultima IV as the apparatus.
- Scanning electron microscopy (SEM) was used to obtain the surface images of the different films.
- UV–Visible spectroscopy was used to report on the thin films' optical properties.

RESULTS AND DISCUSSION

Structural Analysis

Using the fabricated perovskite powders, the MAPbX$_3$ (X = Br, Cl, and I) perovskite thin films were deposited on the FTO using the one-step spin-coating method. The results of the XRD analysis of the deposited films are shown in Fig. 3 as peaks located at 2θ diffraction angles corresponding to the crystallographic planes. The diffractogram of the MAPbBr$_3$ thin film (Fig. 3c) gives 2 peaks at $15°$ and $30°$ corresponding to the (100) and (200) planes, respectively, with the main peak being the one located at $15°$ for the (100) plane. These two crystallographic planes show that the MAPbBr$_3$ thin film has a single crystallographic orientation. The XRD results of the MAPbCl$_3$ thin film (Fig. 3b) show 4 peaks located at $26.62°$, $33.84°$, $37.80°$, and $51.55°$ for the (111), (210), (211), and (310) crystallographic planes, respectively. The main peak of the layer is located at $26.62°$ for the (111) plane. It must be said that the MAPbCl$_3$ thin film has several crystallographic orientations, but the main orientation is along the (111) plane. As for the MAPbI$_3$ layer, we see in Fig. 3a 6 peaks at angles $14.22°$, $24.60°$, $28.55°$, $31.82°$, $33.73°$, and $40.73°$, corresponding, respectively, to the (110), (112), (220), (310), (132), and (141) planes. The major peak is located at $14.22°$ for the (110) plane giving the preferred crystallographic orientation of the MAPbI$_3$ layer. The good resolution of the different peaks and their non-duplication shows that the layers are single-phase and that there are no interstitial defects. Therefore, we can say that the prepared powders have the crystal structure of perovskites.

The value of the lattice parameter, a, determined from the XRD pattern has been calculated using:[75]
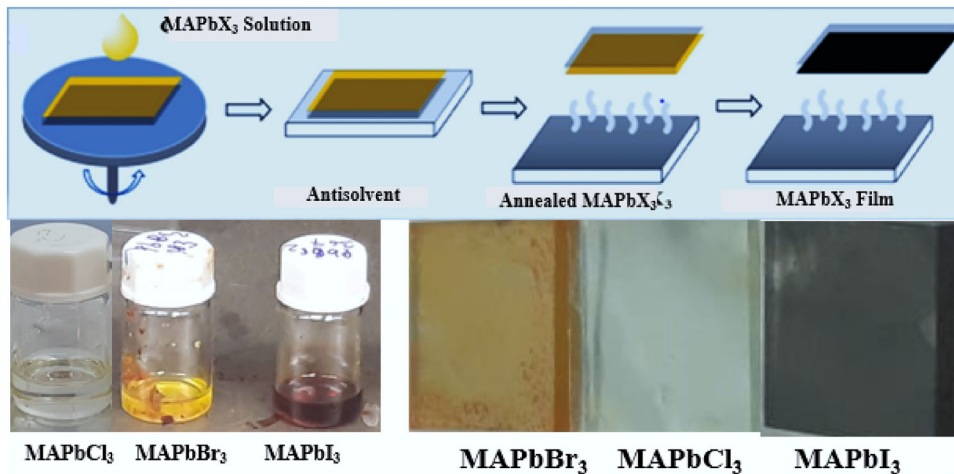
$$a = d_{hkl}\sqrt{h^2 + k^2 + l^2}$$

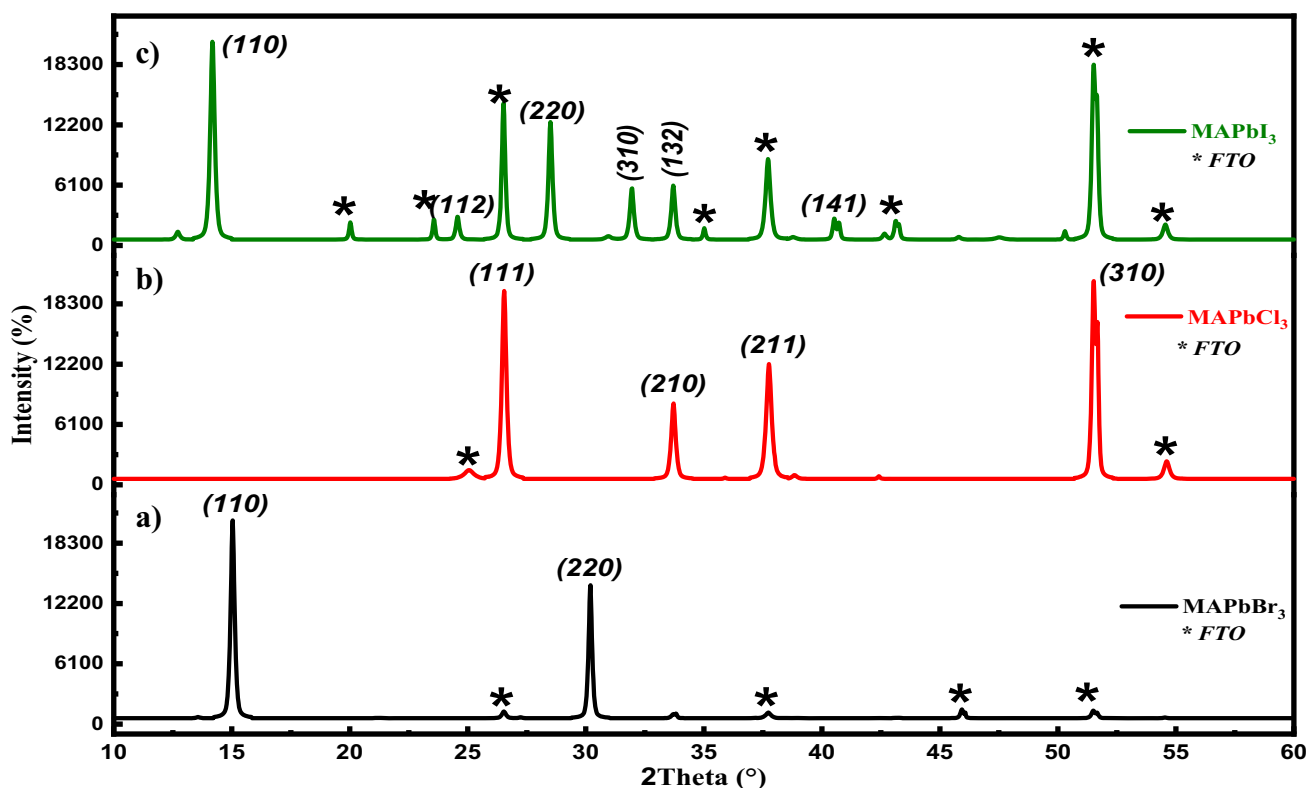Fig 2. The perovskite thin film deposition steps.

Fig 3. XRD diagrams of thin films: (a) MAPbI$_3$, (b) MAPbCl$_3$, and (c) MAPbBr$_3$.

The values for the planes closely match with the 5.41 Å reported in ICDD PDF 65-1691.

The perovskites have a cubic structure with the lattice parameter a = 5.41 Å.

Morphological Analysis

The analysis of the absorptivity of photovoltaic thin films is very important, as they are used as absorbing layers in solar cells. The larger the grain size, the better the surface of the layer, because this means that the surface is less smooth and therefore rough. This roughness favors the trapping of light in order to lower the reflection coefficient. Figure 4 shows the surface images of the thin films that were developed. The size of the grains on the surface of the layers varies. We have well-covered, dense surfaces without voids or cracks, which corresponds to the desired surface. For the MAPbCl$_3$ thin film (Fig. 4b), the grain size is much smaller than for the MAPbBr$_3$ (Fig. 4a) and MAPbI$_3$ (Fig. 4c) films. According to Fig. 4, the grain size for the layers with Br$_3$ and I$_3$ are similar.

Energy dispersive X-ray spectroscopy (EDS) shows the chemical composition of the MAPbBr$_3$, MAPbCl$_3$, and MAPbI$_3$ thin films. Analysis of the sputtered MAPbBr$_3$ film (Fig. 4d) reveals the presence of carbon (c), nitrogen (N), lead (Pb), and bromine (Br) atoms. The presence of iodine (I) and chlorine (Cl) as well as other elements is confirmed by EDS analysis, as shown in Fig. 4e and f. The

formation of thin films depends not only on the stoichiometry of the precursor ratio but also on the deposition conditions such as temperature and substrate, as indicated in previous work.[76,77]

For a detailed distribution, we performed elemental mapping of the MAPbBr$_3$, MAPbCl$_3$, and MAPbI$_3$ thin films, as shown in Fig. 4d, e, and f, respectively. The composite image indicates a good distribution of the elements.

Optical Absorption Spectrum

Photovoltaic thin films are used as absorbing layers in solar cells. Therefore, it is important to characterize the UV–Visible absorption. Figure 5a shows the different absorptions of the MAPbBr$_3$, MAPbI$_3$, and MAPbCl$_3$ layers. From the absorption curves, it can be seen that the MAPbI$_3$ layer has the best absorption, which is probably due to its black dye. The lowest absorption is for the MAPbCl$_3$ layer, also due to its light coloring, which is in line with the results in the literature.[60,61] The various thin films absorb most at 300 nm and this absorption remains virtually constant over the rest of the spectrum.

We can see that the absorption is linked to the dyeing (color) of the thin films. In fact, the darker the film, the more light it absorbs. It is therefore easy to understand why MAPbI$_3$, the darkest film, has the highest absorption. Similarly, MAPbCl$_3$ is
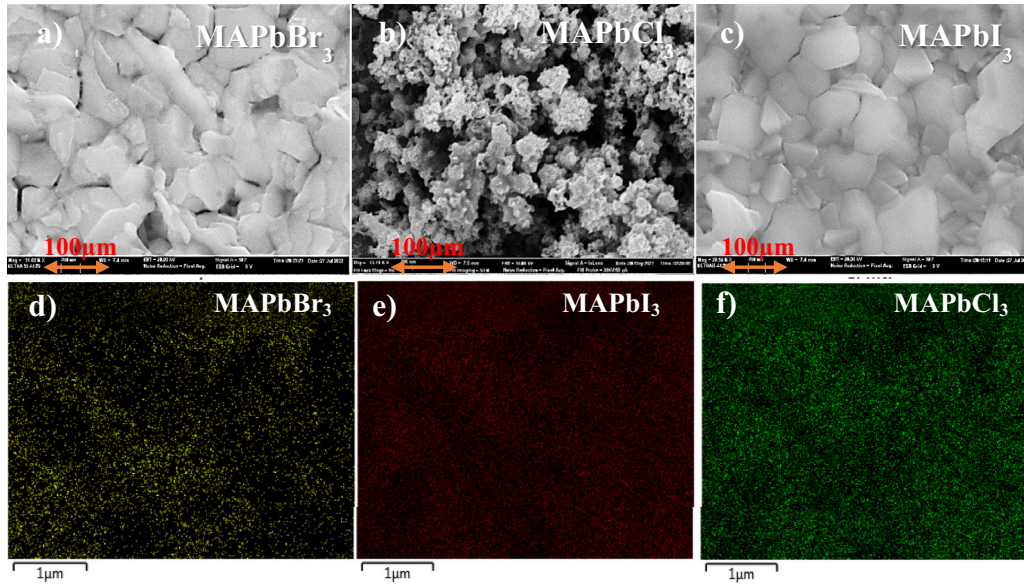
Fig 4. Surface images of perovskite thin films with a magnification of 100 μm: (a) MAPbBr$_3$, (b) MAPbCl$_3$, and (c) MAPbI$_3$. EDS images of perovskite thin films: (d) MAPbBr$_3$, (e) MAPbCl$_3$, and (f) MAPbI$_3$.
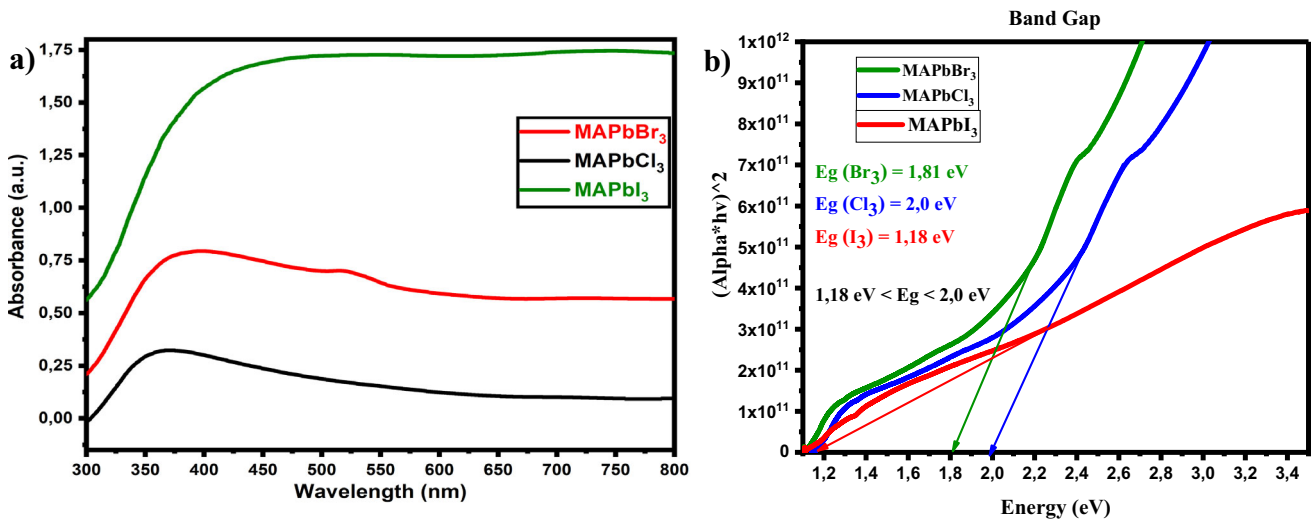

Fig 5. (a) Thin film absorption diagrams, and (b) band gap diagrams.

the lightest thin film in the samples, which gives it the lowest absorption.

As the role of photovoltaic perovskite thin films is to generate electron–hole pairs, it is more important to know their exciton generation capacity. The band gaps of engineered thin films evolve in the opposite direction to the absorption in the wavelength range of 300–400 nm. In this range of the spectrum, the higher the absorption, the smaller the band gap. It can therefore be concluded that, for the processed samples, the effective photons have a wavelength, λ, of less than 300–400 nm.

We have therefore calculated the band gaps of the layers to see which layer best produces charge carriers (electron–hole pairs), based on the wavelengths and absorption coefficients, and these are

shown in Fig. 5b. In this study, we note that the band gaps are in the same direction as the absorptions, i.e., the more the layer absorbs, the more easily it produces electron–hole pairs. The best layer in terms of absorption and taking into account the band gap is the MAPbI$_3$ layer. As for the MAPbBr$_3$ layer, it remains about average while the MAPbCl$_3$ layer has the highest band gap. The band gap values are smaller than those found in the literature, especially for the MAPbI$_3$ layer.[78] This decrease in the band gap of thin films is probably due to the higher purity of the powders used for their preparation.

Table I shows a comparative study of the properties of the samples produced and the literature.

Table I. Comparison of the properties of the three samples produced with those in the literature

Samples	E_g (eV)	Literature E_g (eV), [Ref.]	XRD	Literature XRD, [Ref.]
MAPbI$_3$	1.18	1.66[79]	(110) 14.22° (220) 28.55°	(110) 14.00°[80] (220) 28.30°[80]
MAPbBr$_3$	1.81	2.65[79]	(110) 15.00° (220) 30.00°	(110) 14.00°[80] (220) 28.30°[80]
MAPbCl$_3$	2.00	3.37[79]	(210) 33.84° (211) 37.80° (310) 51.55°	(110) 14.00°[81] (210) 31.80°[81] (211) 35.00°[81]

CONCLUSION

The preparation of the powders was a success, and this method of powder preparation presents itself as an alternative solution to the shortage of perovskite precursors for the manufacture of photovoltaic solar cells. Given the success of the preparation of the MAPbBr$_3$, MAPbCl$_3$, and MAPbI$_3$ powders, we can do the same for other perovskites, such as formamidinium-based perovskites (FAPbX$_3$ with X = Br, Cl, and I), cesium-based perovskites (CsPbX$_3$), or other perovskites. The different thin films elaborated from these prepared powders are of good quality, as shown by the characterization results. X-ray diffraction has allowed us to obtain well-resolved peaks and to confirm the crystal structure of the perovskites. The surface images obtained by scanning electron microscopy showed well-coated surfaces with variable grain sizes. The evaluation of the UV-Visible absorptivity of the thin films leads to the conclusion that the thin films have good absorptivity to be used as absorbing layers in photovoltaic solar cells, especially the MAPbI$_3$ and MAPbBr$_3$ layers. Given the optoelectronic properties of the various thin films developed, we can say that they are well-suited for use in photovoltaic solar cells.

ACKNOWLEDGEMENTS

FUNDING

DATA AVAILABILITY

The data used to support the findings of this study are included in the paper.

CONFLICT OF INTEREST

The authors declare that they have no known competing financial or personal interests.

OPEN ACCESS

REFERENCES

1. D. Gielen, F. Boshell, D. Saygin, M.D. Bazilian, N. Wagner, and R. Gorini, *Energy Strategy Rev.* 24, 38 (2019).
2. J. West, I. Bailey, and M. Winter, *Energy Policy* 38(10), 5739 (2010).
3. T.H. Oh, S.Y. Pang, and S.C. Chua, *Renew. Sustain. Energy Rev.* 14(4), 1241 (2010).
4. S. Jacobsson and A. Johnson, *Energy Policy* 28(9), 625 (2000).
5. I. Dincer, *Renew. Sustain. Energy Rev.* 4(2), 157 (2000).
6. P.A. Owusu and S. Asumadu-Sarkodie, *Cogent Eng.* 3(1), 1167990 (2016).
7. D. Akinwande, C. Huyghebaert, C.H. Wang, M.I. Serna, S. Gossens, L.J. Li, and F.H. Koppens, *Nature* 573(7775), 507 (2019).
8. H. Chfii, A. Bouich, B.M. Soucase, and M. Abd-Lefdil, *Mater. Chem. Phys.* 306, 128006 (2023).
9. H. Chfii, A. Bouich, A. Andrio, J.C. Torres, B.M. Soucase, P. Palacios, M.A. Lefdil, V. Compañ, *Nanomater.*, 13(16), 2312 (2023).
10. C.G. Hwang, in *2006 International Electron Devices Meeting* (IEEE, 2006), pp. 1–8.
11. B. Szelag, K. Hassan, L. Adelmini, E. Ghegin, P. Rodriguez, F. Nemouchi, and S. Olivier, *IEEE J. Sel. Top. Quantum Electron.* 25(5), 1 (2019).
12. A.A. Istratov, H. Hieslmair, and E.R. Weber, *Appl. Phys. A* 70, 489 (2000).
13. E. Maine and E. Garnsey, *Res. Policy* 35(3), 375 (2006).
14. A. Gambardella and A.M. McGahan, *Long Range Plan.* 43(2–3), 262 (2010).

15. M.C. Langley, M.E. Prendergast, and K.M. Grillo, *Archaeol. Anthropol. Sci.* 11, 1 (2019).
16. S. Abdinia, M. Benwadih, E. Cantatore, I. Chartier, S. Jacob, L. Maddiona, and A.H. van Roermund, in *2012 Proceedings of the ESSCIRC (ESSCIRC)* (IEEE, 2012), pp. 145–148.
17. T.J. Welgemoed and C.F. Schutte, *Desalination* 183(1–3), 327 (2005).
18. Z. Liu, R. Mi, G. Ji, Y. Liu, P. Fu, S. Hu, and Z. Xiao, *Ceram. Int.* 47(23), 32634 (2021).
19. H.M. Chen, C. Maohua, and S. Adams, *Phys. Chem. Chem. Phys.* 17(25), 16494 (2015).
20. P. Gao, M. Grätzel, and M.K. Nazeeruddin, *Energy Environ. Sci.* 7(8), 2448 (2014).
21. Q. Tao, P. Xu, M. Li, and W. Lu, *npj Comput. Mater.* 7(1), 23 (2021).
22. F. Igbari, Z.K. Wang, and L.S. Liao, *Adv. Energy Mater.* 9(12), 1803150 (2019).
23. R.E. Brandt, V. Stevanović, D.S. Ginley, and T. Buonassisi, *MRS Commun.* 5(2), 265 (2015).
24. H.J. Snaith, *J. Phys. Chem. Lett.* 4(21), 3623 (2013).
25. N. Yan, C. Zhao, S. You, Y. Zhang, and W. Li, *Chin. Chem. Lett.* 31(3), 643 (2020).
26. Q. Dong, Y. Shi, K. Wang, Y. Li, S. Wang, H. Zhang, and T. Ma, *J. Phys. Chem. C* 119(19), 10212 (2015).
27. S.K. Sahoo, B. Manoharan, and N. Sivakumar, in *Perovskite Photovoltaics* (Academic Press, 2018), pp. 1–24.
28. W.J. Yin, T. Shi, and Y. Yan, *Adv. Mater.* 26(27), 4653 (2014).
29. A. Bouich, J. Marí-Guaita, B. Sahraoui, P. Palacios, and B. Marí, *Front. Energy Res.* 10, 840817 (2022).
30. D. Ginley, M.A. Green, and R. Collins, *MRS Bull.* 33(4), 355 (2008).
31. A. Bouich, J. Marí-Guaita, A. Bouich, I.G. Pradas, and B. Marí, *Eng. Proc.* 12, 81 (2022).
32. W.T. Xie, Y.J. Dai, R.Z. Wang, and K. Sumathy, *Renew. Sustain. Energy Rev.* 15(6), 2588 (2011).
33. A. Bouich, B. Mari, L. Atourki, S. Ullah, and M.E. Touhami, *JOM* 73(2), 551 (2021).
34. A. Bouich, J. Marí-Guaita, A. Bouich, I.G. Pradas, and B. Marí, *Eng. Proc.* 12(1), 81 (2022).
35. T.N. Anderson, M. Duke, G.L. Morrison, and J.K. Carson, *Sol. Energy* 83(4), 445 (2009).
36. J. Zhao, Z. Li, M. Wang, Q. Wang, and Z. Jin, *J. Mater. Chem. A* 9(10), 6029 (2021).
37. Y. Cheng and L. Ding, *SusMat* 1(3), 324 (2021).
38. L. Chao, T. Niu, W. Gao, C. Ran, L. Song, Y. Chen, and W. Huang, *Adv. Mater.* 33(14), 2005410 (2021).
39. J. Cheng, F. Liu, Z. Tang, and Y. Li, *Energy Technol.* 9(8), 2100204 (2021).
40. J.C. Yu, J.H. Park, S.Y. Lee, and M.H. Song, *Nanoscale* 11(4), 1505 (2019).
41. S.A. Veldhuis, P.P. Boix, N. Yantara, M. Li, T.C. Sum, N. Mathews, and S.G. Mhaisalkar, *Adv. Mater.* 28(32), 6804 (2016).
42. H. Cho, Y.H. Kim, C. Wolf, H.D. Lee, and T.W. Lee, *Adv. Mater.* 30(42), 1704587 (2018).
43. Y. Zou, L. Cai, T. Song, and B. Sun, *Small Sci.* 1(8), 2000050 (2021).
44. K. Zhang, N. Zhu, M. Zhang, L. Wang, and J. Xing, *J. Mater. Chem. C* 9(11), 3795 (2021).
45. C.Y. Chang, A.N. Solodukhin, S.Y. Liao, K.P.O. Mahesh, C.L. Hsu, S.A. Ponomarenko, and Y.C. Chao, *J. Mater. Chem. C* 7(28), 8634 (2019).
46. D.B. Potter, D.S. Bhachu, M.J. Powell, J.A. Darr, I.P. Parkin, and C.J. Carmalt, *Phys. Status Solidi (a)* 213(5), 1346 (2016).
47. A.N. Banerjee and K.K. Chattopadhyay, *Prog. Cryst. Growth Charact. Mater.* 50(1–3), 52 (2005).
48. J. Müller, B. Rech, J. Springer, and M. Vanecek, *Sol. Energy* 77(6), 917 (2004).
49. A. Bouich, J. Marí-Guaita, B.M. Soucase, and P. Palacios, *Mater. Res. Bull.* 163, 112213 (2023).
50. A. Bouich, J.C. Torres, H. Chfii, J. Marí-Guaita, Y.H. Khattak, F. Baig, and P. Palacios, *Sol. Energy* 250, 18 (2023).
51. S. Bouazizi, A. Bouich, W. Tlili, M. Amlouk, A. Omri, and B. Soucase, *J. Mol. Gr. Model.* 122, 108458 (2023).
52. A. Bouich. Doctoral dissertation, Universitat Politècnica de València (2021).
53. Y. Ahn, Y. Jeong, and Y. Lee, *ACS Appl. Mater. Interfaces* 4(12), 6410 (2012).
54. L.J. Brennan, M.T. Byrne, M. Bari, and Y.K. Gun'ko, *Adv. Energy Mater.* 1(4), 472 (2011).
55. S.C. Dixon, D.O. Scanlon, C.J. Carmalt, and I.P. Parkin, *J. Mater. Chem. C* 4(29), 6946 (2016).
56. C.L. Hsu and S.J. Chang, *Small* 10(22), 4562 (2014).
57. R. Woods-Robinson, D. Broberg, A. Faghaninia, A. Jain, S.S. Dwaraknath, and K.A. Persson, *Chem. Mater.* 30(22), 8375 (2018).
58. J. Shi, J. Zhang, L. Yang, M. Qu, D.C. Qi, and K.H. Zhang, *Adv. Mater.* 33(50), 2006230 (2021).
59. G.V. Naik, V.M. Shalaev, and A. Boltasseva, *Adv. Mater.* 25(24), 3264 (2013).
60. V.D. Patel and D. Gupta, *Mater. Today Commun.* 31, 103664 (2022).
61. S. Hegedus and A. Luque (eds.), *Handbook of Photovoltaic Science and Engineering* (Wiley, Hoboken, 2011).
62. K. Wang, C. Shao, X. Li, X. Zhang, N. Lu, F. Miao, and Y. Liu, *Catal. Commun.* 67, 6 (2015).
63. I.Y. Bu, *Ceram. Int.* 39(7), 8073 (2013).
64. F. Tian and Y. Liu, *Scr. Mater.* 69(5), 417 (2013).
65. H. Chfii, A. Bouich, B.M. Soucase, and M. Abdlefdil, *Opt. Mater.* 135, 113229 (2023).
66. C.D. Lokhande, A. Ennaoui, P.S. Patil, M. Giersig, K. Diesner, M. Muller, and H. Tributsch, *Thin Solid Films* 340(1–2), 18 (1999).
67. M. Seul and M.J. Sammon, *Thin Solid Films* 185(2), 287 (1990).
68. W. Li, J. Fan, J. Li, Y. Mai, and L. Wang, *J. Am. Chem. Soc.* 137(32), 10399 (2015).
69. A. Dualeh, P. Gao, S.I. Seok, M.K. Nazeeruddin, and M. Grätzel, *Chem. Mater.* 26(21), 6160 (2014).
70. J.S. Manser, M.I. Saidaminov, J.A. Christians, O.M. Bakr, and P.V. Kamat, *Acc. Chem. Res.* 49(2), 330 (2016).
71. M. Spalla, E. Planes, L. Perrin, M. Matheron, S. Berson, and L. Flandin, *ACS Appl. Energy Mater.* 2(10), 7183 (2019).
72. C. Quarti, E. Mosconi, J.M. Ball, V. D'Innocenzo, C. Tao, S. Pathak, and F. De Angelis, *Energy Environ. Sci.* 9(1), 155 (2016).
73. H. Fujimoto, *Carbon* 41(8), 1585 (2003).
74. R.P. Khatri and A.J. Patel, *Int. J. Res. Appl. Sci. Eng. Technol.* 6(3), 1705 (2018).
75. A.M.S. Arulanantham, S. Valanarasu, A. Kathalingam, M. Shkir, and H.S. Kim, *Appl. Phys. A* 124(11), 1 (2018).
76. T. Sall, M. Mollar, and B. Marí, *J. Mater. Sci.* 51(16), 7607 (2016).
77. R.J. Sutton, G.E. Eperon, L. Miranda, E.S. Parrott, B.A. Kamino, J.B. Patel, and H.J. Snaith, *Adv. Energy Mater.* 6(8), 1502458 (2016).
78. D. Zhao, Y. Yu, C. Wang, W. Liao, N. Shrestha, C.R. Grice, and Y. Yan, *Nat. Energy* 2(4), 1 (2017).
79. E. Vega, M. Mollar, and B. Marí, *Phys. Status Solidi (c)* 13(1), 30 (2016).
80. S. Wang, L.K. Ono, M.R. Leyden, Y. Kato, S.R. Raga, M.V. Lee, and Y. Qi, *J. Mater. Chem. A* 3(28), 14631 (2015).
81. P. Pistor, J. Borchert, W. Fränzel, R. Csuk, and R. Scheer, *J. Phys. Chem. Lett.* 5(19), 3308 (2014).